Available online at www.sciencedirect.com
ScienceDirect
Acta Materialia 55 (2007) 1067–1081
Acta MATERIALIA
www.actamat-journals.com

Primary creep in single crystal superalloys: Origins, mechanisms and effects

C.M.F. Rae [a], R.C. Reed [b,*]

[a] Department of Materials Science and Metallurgy, University of Cambridge, Pembroke Street, Cambridge CB2 3QZ, UK
[b] Department of Materials, Imperial College London, Prince Consort Road, London SW7 2BP, UK

Received 21 July 2006; received in revised form 18 September 2006; accepted 18 September 2006
Available online 5 December 2006

Abstract

Creep deformation of the CMSX-4 nickel-base single crystal superalloy is studied in the range 750–850 °C. Emphasis is placed on elucidating the factors causing primary creep when the tensile stress is orientated within 20 °C of the technologically important ⟨0 0 1⟩ direction. It is demonstrated unambiguously that primary creep occurs only if a threshold stress of approximately 500 MPa is exceeded; thereafter the accumulated primary creep strain is proportional to the magnitude by which the threshold stress is surpassed. A very high dependence of the strain rate on the applied stress is observed. Transmission electron microscopy confirms that the stress threshold is associated with the movement of $a\langle 1\,1\,\bar{2}\rangle$ dislocation ribbons through the γ' precipitates by so-called stacking fault shearing. The conditions necessary for the nucleation and propagation of $a\langle 1\,1\,\bar{2}\rangle$ dislocation ribbons and the cessation of their movement are considered; it is demonstrated that the anisotropy of creep deformation for tensile loading within 20 °C of ⟨0 0 1⟩ can be rationalised.

Keywords: Nickel; Single crystal superalloys; Creep deformation; Transmission electron microscopy

1. Introduction

The use of nickel-based single crystal superalloys for the turbine blades in the gas turbines employed for jet propulsion and electricity generation has yielded significant improvements in engine performance, fuel consumption and component efficiencies [1]. Operating conditions are now such that the temperature of the gas stream passing over the blades can be several hundred degrees higher than the melting temperature of a typical alloy [2]. Under these conditions, elaborate cooling channels are needed to moderate the metal temperature. This leads to significant temperature gradients and consequent redistribution of the tensile loading to the cooler webs within the blade. For an aeroengine, this is particularly the case during take-off and climb of the aircraft; for this situation detailed calculations [3] indicate that the stress and temperature conditions are such that a significant degree of primary creep strain can occur. As operating conditions become ever more aggressive, it is becoming increasingly necessary to gain a fundamental appreciation of the deformation modes to be expected of these materials in these situations as they get pushed closer to the limits of their capability.

In this paper, the primary creep of a typical single crystal superalloy is studied as a function of stress and crystallographic orientation. The CMSX-4 alloy is considered on account of its considerable commercial importance. Due to its technological relevance, tensile loading close to ⟨0 0 1⟩ is considered, since this direction is inherited from the investment casting process used for the fabrication of the turbine blades. Experiments reported in the literature [4,5] indicate that when primary creep is initiated in the temperature range 750–850 °C under stresses of perhaps 500 MPa or greater, the micromechanism of creep is quite different from that which occurs at higher temperatures and lower stresses – when dislocation activity is restricted to the matrix (face-centered cubic, γ) channels surrounding the

* Corresponding author.
E-mail address: roger.reed@imperial.ac.uk (R.C. Reed).

1359-6454/$30.00
doi:10.1016/j.actamat.2006.09.026

precipitates ($L1_2$, γ') and is of the $a/2\langle 1\,1\,0\rangle\{1\,1\,1\}$ form [6–8]. Instead, during the primary creep process of interest here, it is well established that deformation occurs by the shearing of the γ' particles by dislocation ribbons of overall Burgers vector $a\langle 1\,1\,2\rangle$ [4,5]. Unfortunately, at this stage the factors promoting the movement of $a\langle 1\,1\,2\rangle$ ribbons are not well understood; neither is the strong creep anisotropy which is displayed for tensile deformation close to the $\langle 0\,0\,1\rangle$ direction [9]. For this reason, attention is focused here on the conditions of stress and orientation which are conducive to the operation of this so-called "stacking fault shear". The micromechanical factors which are responsible for its occurrence are rationalised.

2. Background

The seminal paper on primary creep in single crystal superalloys is due to Leverant and Kear [10], who studied the creep performance of the alloy Mar-M200 at 760 °C and 750 MPa, i.e. in the low-temperature, high-stress regime. Creep testing was carried out on specimens of orientation close to [0 0 1]; it was demonstrated that, even though the tensile axes of the cylindrical testpieces examined were within 18 °C of the [0 0 1] pole, the primary creep strain could vary from test to test by up to a factor of seven. Transmission electron microscopy confirmed the presence – along with the expected $a/2\langle 1\,1\,0\rangle$ dislocations in the matrix phase γ – of dislocation ribbons of overall Burgers vector $a\langle 1\,1\,2\rangle$ dissociated into superlattice partial dislocations separated by intrinsic and extrinsic stacking faults. The ribbons were seemingly able to cut through the γ' phase without leaving dislocation debris at the γ/γ' interfaces. By examining the rotation of the tensile axis and the dominant slip plane traces, both of which were clearly characteristic of $a\langle 1\,1\,2\rangle\{1\,1\,1\}$ slip, these dislocation ribbons were confirmed as the major cause of the deformation strain. The extent of primary creep was found to correlate well with the delayed operation of secondary slip systems: the best creep performance came from orientations of tensile axes near [0 0 1], where four slip systems are identically stressed and along the [0 0 1]–[0 1 1] symmetry boundary where two systems are equally favoured. An image of a dislocation ribbon in a modern single crystal superalloy is given in Fig. 1; it is strikingly similar to that given in Fig. 7 of the Leverant and Kear paper [10].

Subsequently, the range of orientations studied was greatly extended by MacKay and Meier [11], who tested not only Mar-M200 but also Mar-M247 in the primary creep regime in which the γ' particles were sheared, the conclusions drawn being in close agreement with those of Leverant and Kear [10]. These two alloys are representative of the very first generation of nickel-base single crystal superalloys to be designed. This paper presented a diagram ranking the creep resistance of the various orientations within one standard triangle of the sterogram, see Fig. 2, which has been reproduced subsequently many times. It indicates that orientations towards the right-hand side of the triangle

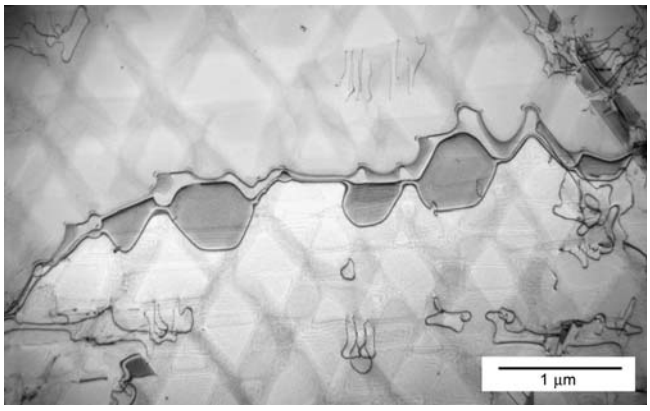

Fig. 1. Transmission electron micrograph of a $a\langle 1\,1\,\bar{2}\rangle$ ribbon in the single crystal superalloy TMS-82+, deformed in creep at 750 °C and 750 MPa to 11% strain. The foil normal is {1 1 1}.

(between [0 1 1] and $[\bar{1}\,1\,1]$) show particularly poor creep properties since the two slip systems favoured in these orientations operate on the same slip plane and thus the work-hardening rate is low. For orientations within 20 °C of [0 0 1], the angle of rotation α necessary for the tensile axis to reach the [0 0 1]–[0 1 2] symmetry boundary (as required by $a\langle 1\,1\,2\rangle\{1\,1\,1\}$ deformation) was considered to be the prime determinant of the creep performance – larger values of α promote primary creep [11]. Later studies [5] attempted to rationalise the extent of primary creep in a quantitative fashion using the α parameter, but microstructural evidence [12] revealed that the hardening process is more complex than the simple picture of Ref. [11]: even for specimens oriented for single slip, two or more slip systems operate from an early stage to varying degrees and the transition to secondary creep occurs long before the tensile axis rotates as far as the [0 0 1]–[0 1 2] symmetry boundary. Rae et al. [13] have used the term "stacking fault shear" to describe the movement of the dislocation ribbons, i.e. strongly coupled intrinsic/extrinsic fault pairs of net Burgers vector $a\langle 1\,1\,2\rangle$, through the γ/γ' structure; this terminology will be adopted in this paper.

Since these early studies, much alloy development has been accomplished and compositions consistent with second-, third- and even fourth-generation single crystal superalloys can now be identified [1]. For example, additions of rhenium and ruthenium were introduced in the second- and fourth-generation alloys, respectively. Thus the possibility exists that these new alloys exhibit a sensitivity to stacking fault shear which is subtly different from those of the earlier ones. Indeed, in the well-cited paper of Pollock and Argon [14], which deals with the creep deformation behaviour of CMSX-3 at 825 °C and 450 MPa, no stacking fault shear is reported: the dislocations propagated from grown-in dislocations looping through the channels between the γ' precipitates. Here, it is likely that the stress level was insufficient for the γ' to be penetrated and indeed, consistent with this, little if any primary creep deformation is evident in the creep curves presented. On the other hand, Sass et al. [15] studied the creep of

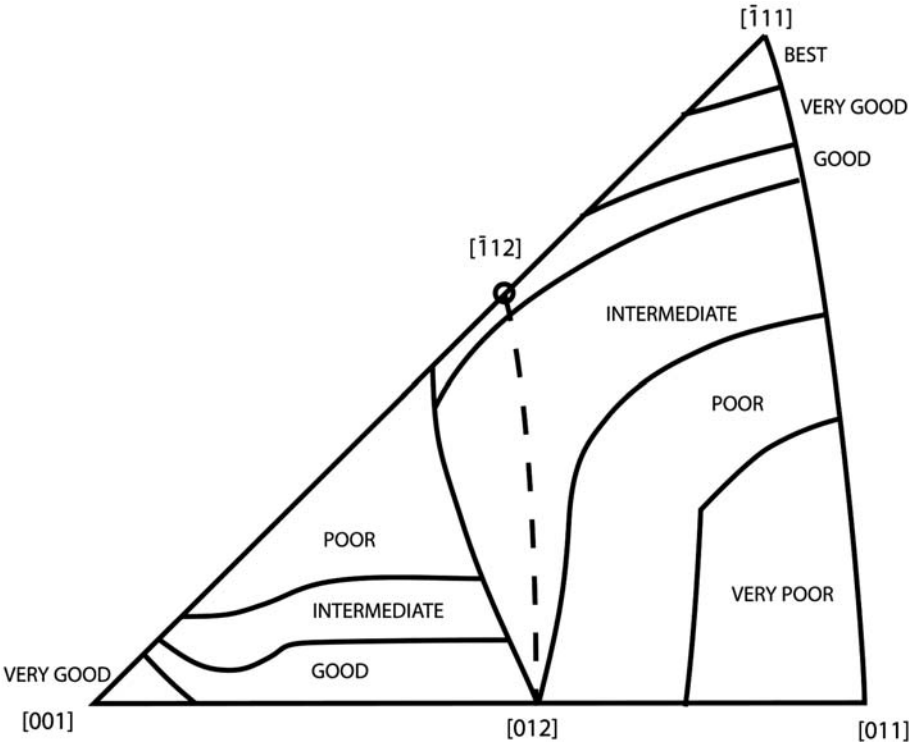

Fig. 2. Orientation dependence of creep performance as described by MacKay and Maier [11].

CMSX-4 at 850 °C and stresses of 500 MPa and 650 MPa and reported that the primary creep behaviour was sensitive to even small misorientations from [0 0 1]; an increase in the density of the stacking faults with higher stress was noted and the authors suggested a change in prevailing mechanism with increasing stress. This confirms to the present authors the need for well-controlled experimentation in which the threshold stress for stacking fault shear is determined on specimens of identical orientation, so that any orientation dependence is removed; this has not been attempted so far. Interestingly, Caron and Kahn [16] demonstrated that reducing the primary γ' size in a number of different single crystal alloys increased the primary creep strain and subsequent secondary creep rates for orientations close to [0 0 1]; microstructural examination showed that low primary creep rates were associated with an homogeneous distribution of dislocations in the γ facilitated by the larger width of the γ channels in the coarser microstructure. A similar observation of greatly increased primary creep was made when secondary γ' precipitates were made to precipitate in the γ channels of the alloy SRR99 [17] and an experimental alloy [18]. More recently, Drew and coworkers [19] have studied second- and third-generation superalloys in primary creep and have demonstrated that the rhenium-containing single crystal superalloys are more prone to stacking fault shear. Reed has attempted a classification of the different creep deformation processes arising in the second-generation superalloy CMSX-4 [1], although it should be noted that the stress levels and temperatures required for the transitions between the different regimes will differ from alloy to alloy.

Given the content of this paper, it is appropriate to consider briefly the current understanding of the mechanism of formation of the $a\langle 1\,1\,\bar{2}\rangle$ dislocation ribbons. This is now known to involve the reaction of $a/2\langle 1\,\bar{1}\,0\rangle\{1\,1\,1\}$ dislocations in γ which are dissociated into their Shockley partials. A typical reaction might then be [5,7,9]

$$a/2[0\,1\,1] + a/2[\bar{1}\,0\,1] \rightarrow a/3[\bar{1}\,1\,2] + a/6[\bar{1}\,1\,2]. \quad (1)$$

If the applied stress is sufficient, then the $a/3[\bar{1}\,1\,2]$ dislocation is able to enter the γ' leaving a superlattice intrinsic stacking fault (SISF) behind it, see Fig. 3(a), and the remaining $a/6[\bar{1}\,1\,2]$ at the γ/γ' interface. Formation of the ribbon in γ' then requires further reactions between the $a/2\langle 1\,\bar{1}\,0\rangle\{1\,1\,1\}$ type dislocations, such that the original $a/6[\bar{1}\,1\,2]$, a further $a/6[\bar{1}\,1\,2]$ and eventually a second $a/3[\bar{1}\,1\,2]$ enter the γ', see Fig. 3(b). An anti-phase boundary (APB) then separates the two $a/6[\bar{1}\,1\,2]$ dislocations, and a superlattice extrinsic stacking fault (SESF) the second $a/6[\bar{1}\,1\,2]$ and the final $a/3[\bar{1}\,1\,2]$. Once formed, the ribbons are able to glide through the γ' precipitates in a glissile fashion, although as noted by Leverant and Kear [10], their motion is most likely to be controlled by diffusion since – if the shearing sequence is to be rationalised – atomic adjustments are required at or near to the core of the first $a/3\langle 1\,1\,\bar{2}\rangle$ partial dislocation as it enters the γ'. Ribbons intersecting a γ' precipitate cause it to be populated with stacking faults, and these are commonly observed in the transmission electron micrographs of specimens subjected to primary creep deformation.

Clearly, the work carried out so far indicates that the occurrence of stacking fault shear is a sensitive function

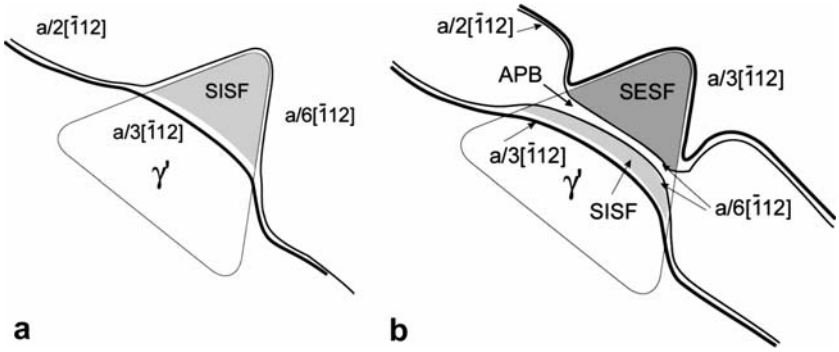

Fig. 3. Illustration of the mechanism of shearing of the γ' by an $a\langle 1\,1\,\bar{2}\rangle$ ribbon during primary creep. An $a/3[\bar{1}\,1\,2]$ dislocation enters the γ' leaving a superlattice intrinsic stacking fault (SISF) behind it (a), leaving an $a/6[\bar{1}\,1\,2]$ partial at the γ/γ' interface. In (b), the original $a/6[\bar{1}\,1\,2]$ and a further $a/6[\bar{1}\,1\,2]$ have entered the γ', leaving an $a/3[\bar{1}\,1\,2]$ partial at the interface.

of both the applied stress and orientation. Unfortunately, the existing picture is confused because comparisons have been made between tests for which both have varied; the relative influences of applied stress and orientation (which seem to be equally potent) cannot therefore be isolated. The mechanism is also potentially a function of the temperature, although it is not clear the extent to which this can be explained through the decreased stress levels at which higher temperature tests are conducted, combined with increased competition from $a/2\langle 1\,\bar{1}\,0\rangle\{1\,1\,1\}$ matrix deformation as dislocation climb mechanisms become prevalent at higher temperatures. The work presented in this paper was conducted with these considerations in mind, and in an effort to rationalise the orientation dependence of the primary creep phenomenon for loading close to the technologically important $\langle 0\,0\,1\rangle$ orientation.

3. Experimental work

The CMSX-4 single crystal material used here was provided by Rolls-Royce plc in the fully heat-treated condition. For the determination of the effect of stress on creep deformation, cylindrical blanks suitable for the machining of testpieces were taken from two single crystal slabs of dimensions 20 cm by 6 cm by 1 cm, see Fig. 4a. For each slab, one of the long axes was aligned nominally along $\langle 0\,0\,1\rangle$. By using material from a single casting it was possible to produce two series of specimens, termed A and B, each of which were matched in orientation, microstructure and composition. Creep strain testpieces of diameter 5.6 mm and gauge length 60 mm were prepared and strain testing carried out using 20 kN constant load creep testing machines; such testing was compliant with the British Standard UDC 629.7 [20]. The plastic (creep) strains reported here were determined after subtracting the elastic strains determined from the incremental loading procedure. The initial orientations of the testpieces were determined by the automatic indexing of back-reflection Laue patterns using the SCORPIO method, which is reviewed in Ref. [21]. The orientations of the specimens determined in this way are plotted on the standard stereographic triangle in Fig. 4b; note that only the $[0\,0\,1]$–$[\bar{1}\,1\,2]$–$[0\,1\,2]$ portion of the full standard triangle of Fig. 2 is considered here and subsequently since orientations within 20 °C of $\langle 0\,0\,1\rangle$ are

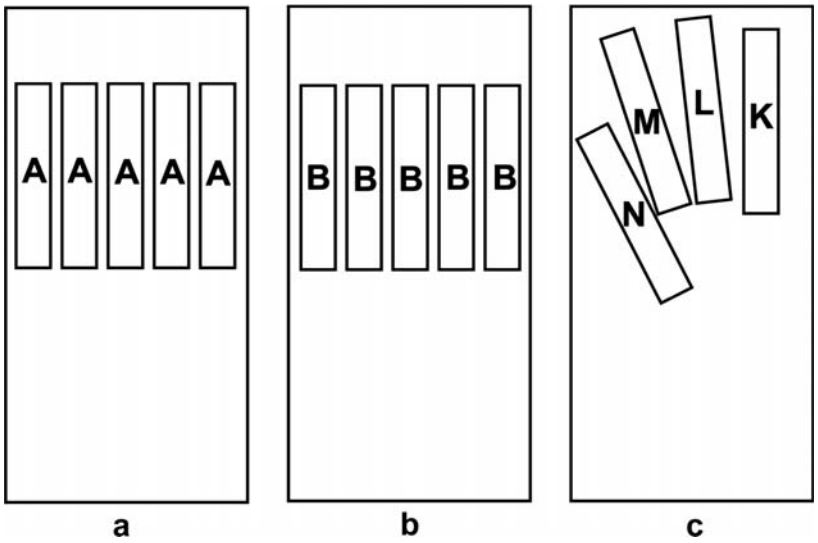

Fig. 4a. Illustration of the strategy used for the machining of testpieces from single crystal slabs of CMSX-4.

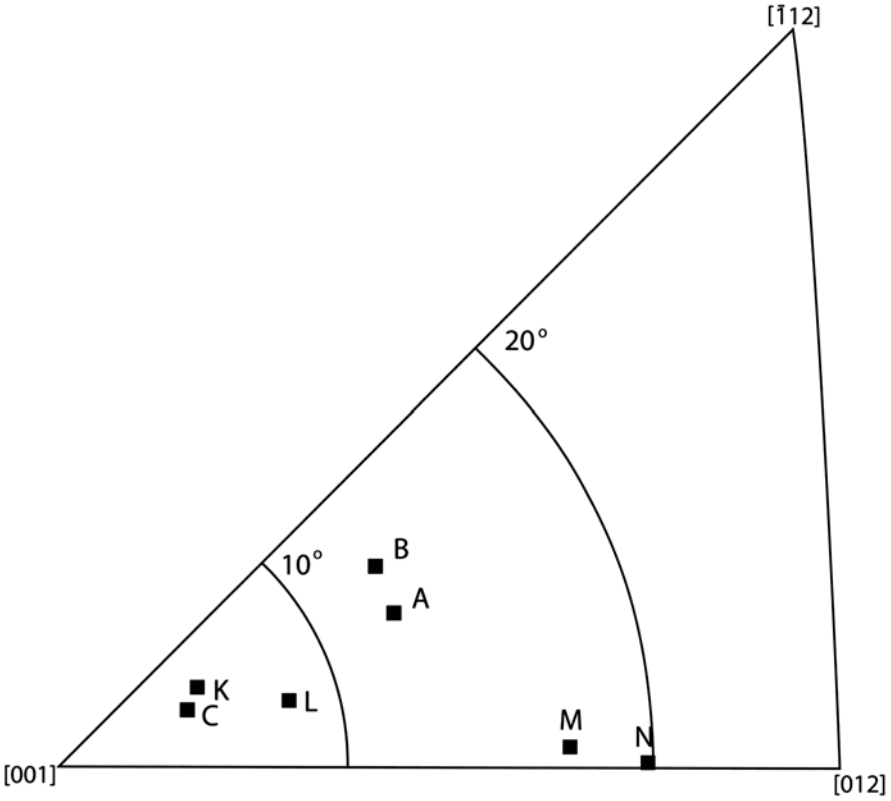

Fig. 4b. Orientations of slabs A and B, specimen C and also K, L, M and N [5], plotted within a portion of a standard triangle of the stereographic projection.

being considered. In the present paper, reference is made also to the results from creep tests carried out on specimens tested at 750 °C and 750 MPa which were machined from a single slab to produce the specimens K, L, M and N, see Fig. 4a, as reported in Ref. [5]. During the course of the work, it became necessary to perform additional testing on one further creep specimen, C, machined from a fully heat-treated cast rod; this had an orientation close to that of specimen K. Crystallographic information about the orientations of the various samples are given in Table 1.

For analysis by transmission electron microscopy, discs were cut from the creep specimens normal to the tensile axis or approximately parallel to a slip plane. After thinning by mechanical abrasion, these were electropolished at 20 V in a solution of 10% perchloric acid in methanol. The resulting foils were examined in a JEOL 2000FX transmission electron microscope operating at 200 kV.

4. Results

The results of creep tests at various levels of stress between 450 and 750 MPa are given in Fig. 5a for the temperature of 750 °C (series A) and in Fig. 5b for 850 °C (series B). It is emphasised again that due to the nature of the

Table 1
Table summarising the extent of primary creep, creep rates, rupture lives, etc., for the tests reported here

	Orientation		Temp./stress	Primary creep (%)	Primary creep rate (s^{-1})	Secondary creep rate $\times 10^{-8}$ s^{-1}	Life hours	Total strain (%)
	θ	ρ						
A	12.7°	24.4°	750 °C/750 MPa	7.0	4.44×10^{-6}	8.00×10^{-8} s^{1}	410 h	23.25
			750 °C/650 MPa	4.1	6.0×10^{-7}	2.78×10^{-9} s^{-1}	(2804 h)	(7.89)
			750 °C/600 MPa	2.1	6.67×10^{-8}	Int	(1996 h)	(3.27)
			750 °C/550 MPa	0.8	4.44×10^{-9}	Int	(665)	(0.73)
			750 °C/450 MPa	0	$\sim 8 \times 10^{-11}$	Int	(1890 h)	(0.044)
B	12.9°	31.3°	850 °C/750 MPa	2.8	4.97×10^{-5}	2.617×10^{-6} s^{-1}	9.88	20.3
			850 °C/650 MPa	2.0	1.34×10^{-5}	2.67×10^{-7} s^{-1}	81.8	20.5
			850 °C/550 MPa	1.2	1.35×10^{-5}	2.83×10^{-8} s^{-1}	517	17.7
			850 °C/500 MPa	0.5	1.57×10^{-7}	2.83×10^{-9} s^{-1}	988	24.5
C	4.7°	23.5	750 °C/500 MPa	Int.	1.66×10^{-6}	Int	(4.2)	(1.4)

For the interrupted tests, the life and strain are in brackets.

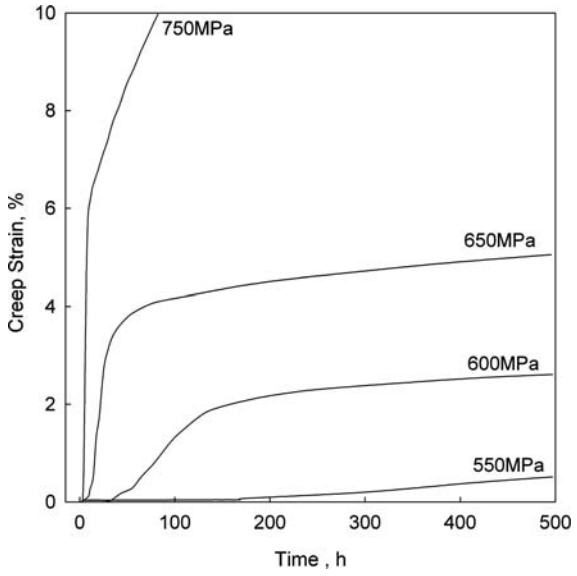

Fig. 5a. Creep curves for CMSX-4 deformed at 750 °C at various magnitudes of applied stress, confirming the absence of primary creep for values less than about 500 MPa.

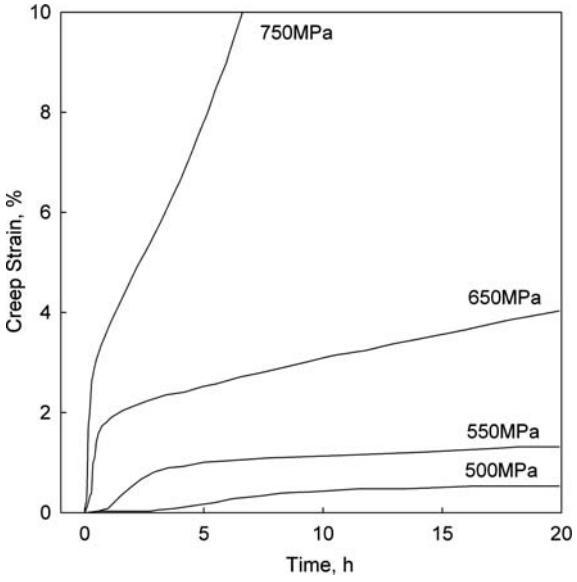

Fig. 5b. Creep curves for CMSX-4 deformed at 850 °C at various magnitudes of applied stress, confirming the absence of primary creep for values less than about 500 MPa.

experimental design, the testpieces can have exhibited no differences in orientation, microstructure and chemistry; thus any differing behaviour is due solely to the magnitude of the applied stress. It can be seen that the extent of primary creep and the primary creep rate both increase rapidly with applied stress, consistent with the experimentation reported in Refs. [22,23]. The amount of primary creep was estimated by extrapolating the maximum primary creep gradient to intersect the minimum secondary creep gradient, as described in Ref. [11]. These data are given in Table 1 together with strain rates and rupture lives. In Fig. 6 the primary creep strain is plotted against

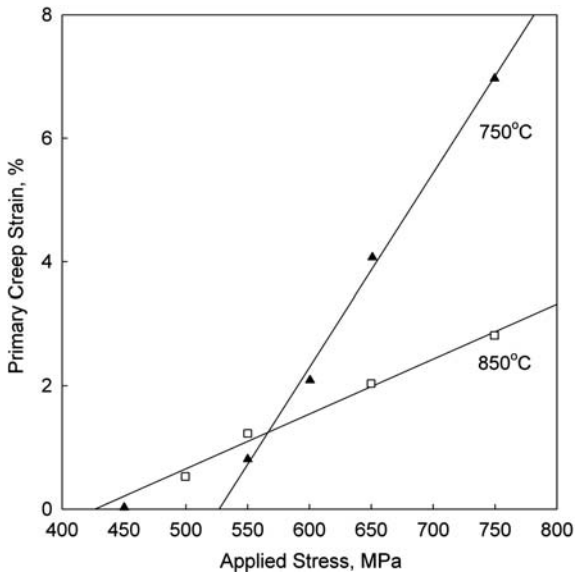

Fig. 6. Extent of primary creep as a function of applied stress.

the applied tensile stress at the two test temperatures. It is seen that the extent of primary creep increases linearly with applied stress once a threshold stress is exceeded; note that at 750 °C, a stress of 450 MPa was insufficient to cause primary creep. Thus the threshold stress is ~530 MPa at 750 °C and ~430 MPa at 850 °C. The stress exponent, n, relating minimum strain rate to stress through the equation $\dot{\epsilon} \propto \sigma^n$ was determined from the gradient of a plot of $\ln\{\dot{\epsilon}\}$ vs. $\ln\{\sigma\}$, see Fig. 7; for this purpose, the minimum strain rates employed corresponded to those in the pseudo-steady-state at larger strains, just prior to failure [23]. A stress exponent of $n = 22$ was found at 750 °C, reducing to 14 at 850 °C – the latter value is comparable to the $n = 13.5$ found for CMSX-4 tested at 800 °C in Ref. [23]. The results of the creep tests can be compared with those of specimens K, L, M and N which were previously

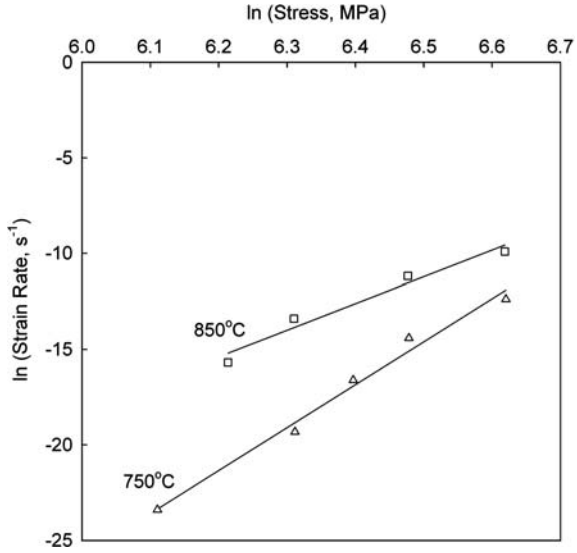

Fig. 7. Plot of the logarithm of strain rate vs. logarithm of stress at 750 °C and 850 °C.

reported [5] and which are given again in Fig. 8; a comparison of the different creep curves makes clear that the accumulated primary creep strain is equally sensitive to changes in orientation and applied stress.

Several of the tests at 750 °C were stopped before rupture in order to examine the microstructure before the cessation of primary creep. Fig. 9 shows the microstructures of specimens deformed to the end of primary creep at 750 MPa (after 8 h) and at 550 MPa (after 670 h). Both show evidence of the formation of stacking faults but the extent to which these have penetrated the γ' varies greatly: at 750 MPa nearly all stacking faults were found to extend fully through the γ', but at 550 MPa the stacking faults rarely (if at all) propagated through the γ' precipitates. The levels of dislocation density at the γ/γ' interface were comparable, consistent with both specimens being at the end of primary creep. Thus the increased activity of the $a\langle 1\,1\,2\rangle\{1\,1\,1\}$ shear mechanism must be associated with the greater stress and thus the high primary creep strain and larger secondary creep rate. The sample tested at 450 MPa displayed a constantly decreasing creep rate and was halted after nearly 1900 h. The microstructure shows some $a/2\langle 1\,1\,0\rangle$ dislocation activity but large areas remain dislocation-free, see Fig. 10.

A further sample C was creep tested to 1.4% strain at 750 °C, 750 MPa and interrupted as the creep rate reached a maximum, approximately halfway through the primary creep stage. The orientation of this specimen was within 6 °C of the [0 0 1] axis and displayed activity on several slip planes, as well as the interactions which lead to hardening. The sample was sectioned close to the primary creep plane. At this stage the deformation microstructure is inhomogeneous: in some areas the dislocation density is low and mobile $a\langle 1\,1\,2\rangle$ ribbons were seen on several planes, in some cases intersecting, e.g. at A, Fig. 11(a). In other areas

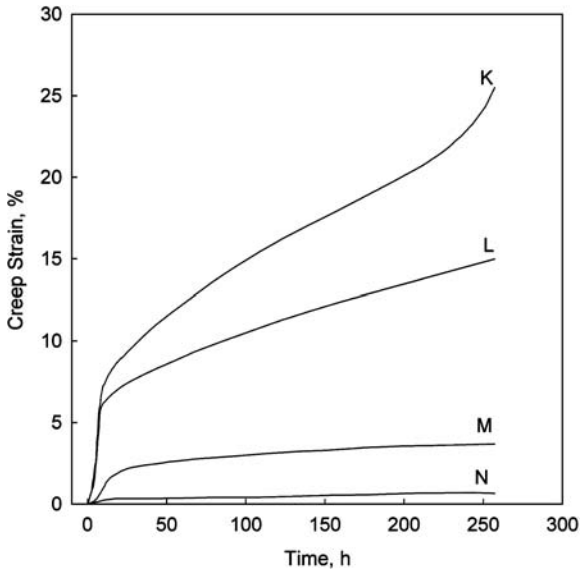

Fig. 8. Creep test results for specimens K, L, M and N tested at 750 °C and 750 MPa [5].

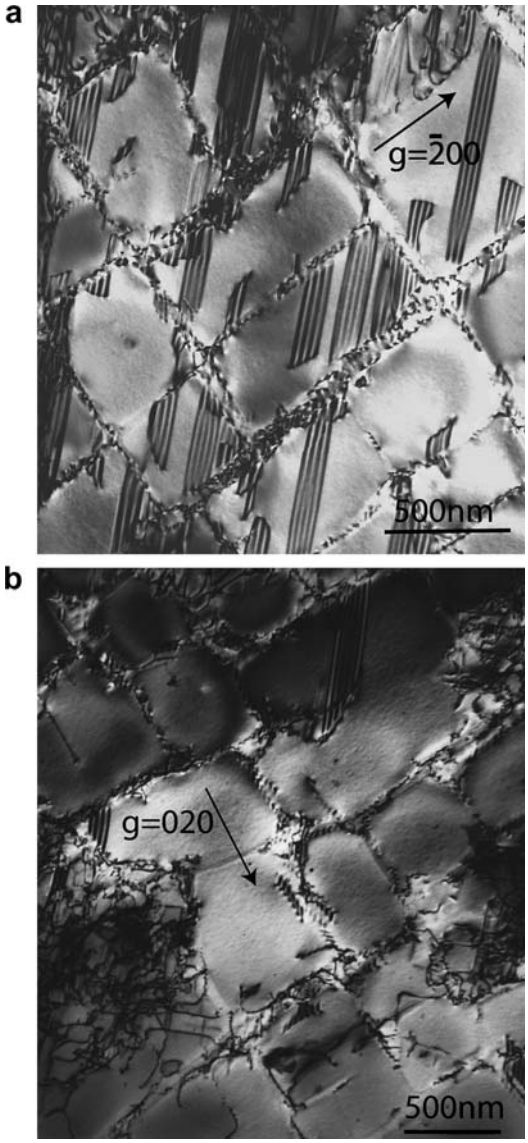

Fig. 9. TEM micrographs of specimens of orientation A deformed to the end of primary creep showing the lack of stacking faults in the γ' at the lower stress: (a) 750 °C/750 MPa, (b) 750 °C/550 MPa.

$a/2\langle 1\,1\,0\rangle$ dislocations progressively filled the horizontal γ channels thus excluding $a\langle 1\,1\,2\rangle$ shear, see Fig. 11(b). Where the density of dislocations in the γ channels was higher, dislocation ribbons were forming on the primary slip plane and moving away, but the density of dislocations at the γ/γ' interface prevented large-scale movement in this area, Fig. 11(c). Note that the horizontal channels fill with the $a/2\langle 1\,1\,0\rangle$ dislocations first. Thus hardening occurs by the interaction of the active $a\langle 1\,1\,2\rangle$ dislocation ribbons and by the propagation of $a/2\langle 1\,1\,0\rangle$ dislocations in the γ which blocks movement of the ribbons. These findings are broadly consistent with observations reported elsewhere [24,25].

The viscous movement of the dislocation ribbon through the γ/γ' structure is illustrated by the defect in Fig. 12: the leading $a/3\langle 1\,1\,2\rangle$ dislocation edge has entered the γ' but, despite the high curvature, is having difficulty

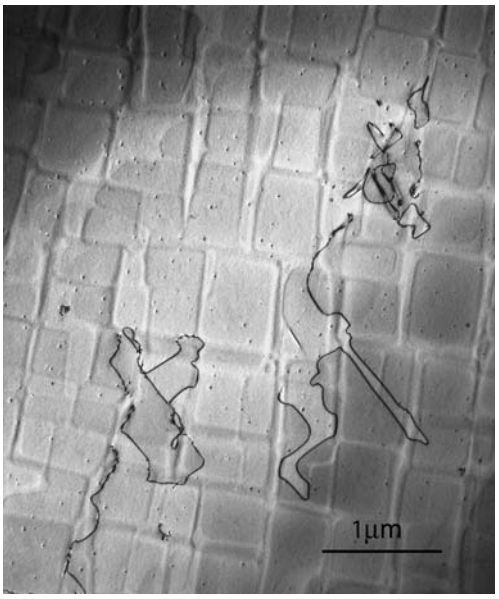

Fig. 10. Deformation microstructure of specimen deformed at 750 °C and 450 °C.

propagating the intrinsic fault. This configuration was commonly displayed.

5. Discussion and interpretation of results

The results demonstrate conclusively that the extent of primary creep is acutely dependent upon the level of applied stress. The primary creep strain increases rapidly once a stress threshold is exceeded. The microstructural observations made using transmission electron microscopy demonstrate that, as the threshold for the occurrence of primary creep is approached, stacking faults are readily formed in the microstructure but do not necessarily propagate into the γ'. The primary creep threshold can be associated, therefore, with the propagation of stacking fault ribbons through the γ and γ'. In the stress range where stacking fault shear can occur, a very rapid increase in strain rate with stress arises.

From these considerations, it is clear that the accumulation of substantial primary creep strain depends upon three distinct conditions being satisfied: (i) the nucleation of the $a\langle 1\,1\,2\rangle$ ribbons from the $a/2\langle 1\,1\,0\rangle$ dislocations which must have formed in the γ matrix; (ii) the successful propagation of the ribbon through the γ/γ' microstructure; and (iii) a degree of work-hardening which allows sufficient time for propagation to occur before the γ channels become clogged with $a/2\langle 1\,1\,0\rangle$ dislocations so that movement of ribbons then becomes impossible. In the following sections, further consideration is given to the details of these processes and calculations are made to put them on a quantitative basis.

5.1. Nucleation of the stacking fault ribbon

Eq. (1) indicates that the nucleation of a stacking fault ribbon will depend upon the availability of suitable

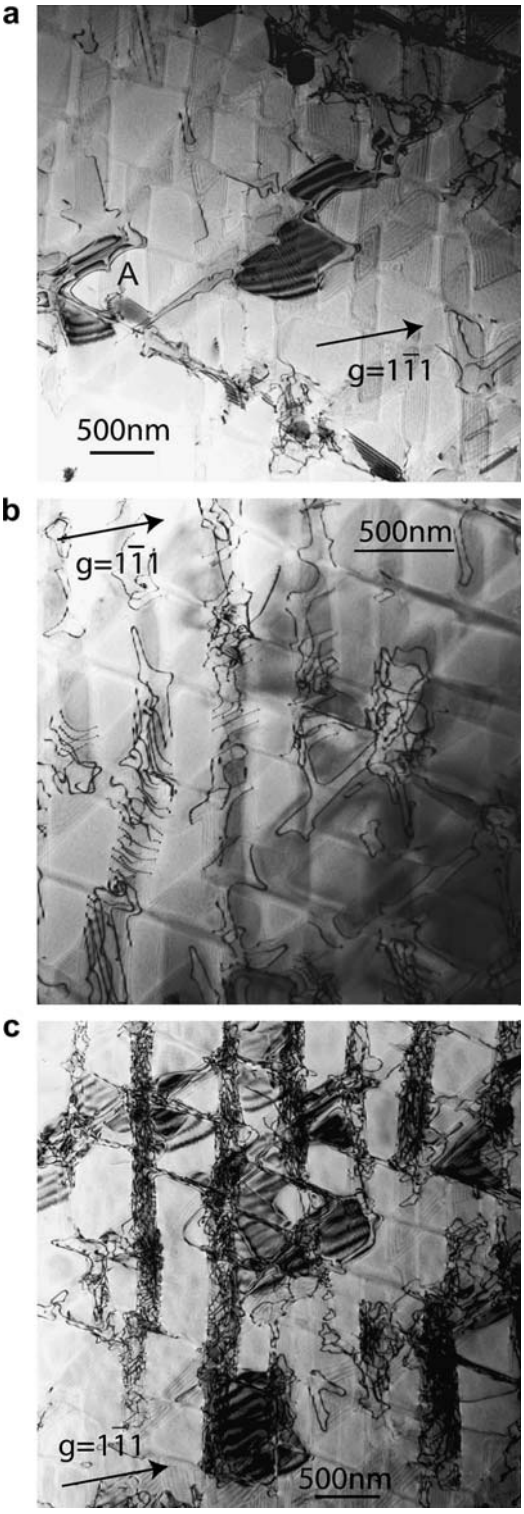

Fig. 11. TEM microstructures of specimen orientation C deformed at 750 °C and 750 MPa and sections close to the primary slip plane: (a) showing $a\langle 1\,1\,2\rangle$ dislocation ribbons moving along in a relatively dislocation-free area with ribbons on two planes colliding; (b) showing movement of $a/2\langle 1\,1\,0\rangle$ dislocations to fill γ channels; and (c) showing dislocations in the γ impeding stacking fault shear.

$a/2\langle 1\,1\,0\rangle\{1\,1\,1\}$ matrix dislocations; where these are unavailable due to low resolved shear stress, or alternatively if the geometry is such that a ribbon of an appropriate

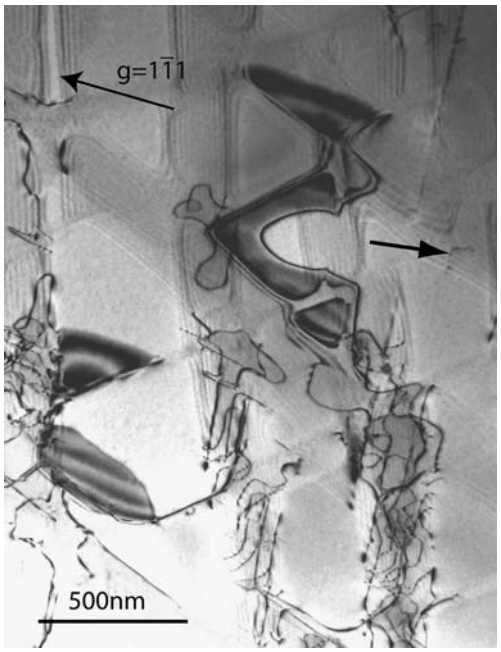

Fig. 12. Dislocation ribbon showing the difficulty of propagating a SISF across the γ' precipitate.

configuration cannot form, then the nucleation of primary creep is not expected. To gauge the effect of these considerations, the resolved shear stress has been calculated on the full range of possible $a/2\langle 1\,1\,0\rangle\{1\,1\,1\}$ slip systems for all orientations within the [0 0 1]–[0 1 2]–[$\bar{1}$ 1 2] triangle of the stereogram. By imposing a stress threshold τ_{110} for $a/2\langle 1\,1\,0\rangle\{1\,1\,1\}$ matrix dislocations to be active, the exact nature of them can be determined as a function of τ_{110} and crystallographic orientation; the nature of the limited number of $a\langle 1\,1\,2\rangle$ dislocation ribbons so produced then follows. The following example helps to reinforce these ideas. Consider the situation when the tensile axis is aligned along the [$\bar{1}$ 1 2] direction; then two slip systems, [$\bar{1}$ 0 1](1 1 1) and [0 1 1]($\bar{1}\,\bar{1}$ 1), have a Schmid factor of 0.408, and all remaining systems have Schmid factors of 0.272 or less. Dislocations from the two highly loaded systems, i.e. [$\bar{1}$ 0 1](1 1 1) and [0 1 1]($\bar{1}\,\bar{1}$ 1), can combine to form the ribbon a[$\bar{1}$ 1 2]($\bar{1}\bar{1}$1); note that it is not necessary for the matrix dislocations to have a common plane in order to combine. The nature of the different $a\langle 1\,1\,2\rangle\{1\,1\,1\}$ ribbons and the types of $a/2\langle 1\,1\,0\rangle\{1\,1\,1\}$ dislocations required to form them are summarised in Fig. 13. Note that the formation of any given

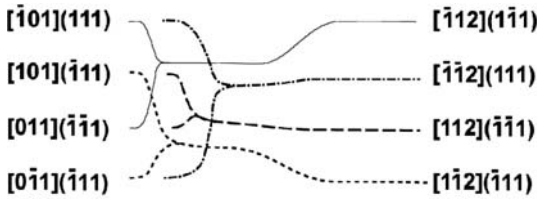

Fig. 13. Summary of the types of $a/2\langle 1\,1\,0\rangle$ dislocations required to form a ribbon of type $a\langle 1\,1\,2\rangle$.

$a\langle 1\,1\,2\rangle\{1\,1\,1\}$ ribbon requires two distinct $a/2\langle 1\,1\,0\rangle\{1\,1\,1\}$ types to be present.

Using calculations made in this way, Fig. 14 confirms the orientations where it is possible to nucleate $a\langle 1\,1\,2\rangle$ ribbons from the active $a/2\langle 1\,1\,0\rangle$ dislocation populations as a function of orientation and applied tensile stress. The value of the stress threshold τ_{110} used in the calculations was 210 MPa: this being the maximum resolved shear stress on the specimen deformed at 750 °C and 450 MPa for which dislocation penetration was relatively slight even after 2000 h. One can see that the orientation for which nucleation of $a\langle 1\,1\,2\rangle\{1\,1\,1\}$ creep is predicted to occur at the lowest applied stress level lies at a point close to [$\bar{1}$ 1 4], along the symmetry line joining [0 0 1] and [$\bar{1}$ 1 2] poles; nucleation is hardest for tensile axes along the [1 1 2] direction. The predictions indicate that ribbon nucleation is easiest along the [0 0 1]–[$\bar{1}$ 1 2] symmetry boundary, and becomed progressively more difficult as the [0 1 2] orientation is approached. Note, however, that the magnitude of the threshold stress τ_{110} must be regarded as approximate and will vary with the γ' volume fraction, γ' size and with misfit and temperature. For example, the threshold value would need to rise to $\sim$235 MPa for orientation N to fall within the zone of no $a\langle 1\,1\,2\rangle$ nucleation at 750 MPa. Pollock and Argon considered the Orowan resistance for the bowing of dislocations in the γ channels and estimated a value of 166 MPa for the alloy CMSX-2. They also noted that a negative γ/γ' misfit will increase the effective stress in the channels normal to the tensile axis. Thus the threshold stress is likely to differ, not just for channels parallel and normal to the tensile axis, but between the dendrite cores and the interdendritic regions since residual microsegregation of rhenium and tantalum causes differences in the γ' volume fraction [26].

These considerations explain the very low primary creep strain and insignificant creep rates displayed by sample N, see Fig. 8, for which stacking fault shear was found to be unable to nucleate from the $a/2\langle 1\,1\,0\rangle\{1\,1\,1\}$ dislocations present in the γ [5]. Within the orientation range [0 1 2]–[0 1 3] Burgers vectors, a/2[1 0 1] and $a/2$[$\bar{1}$ 0 1], were found to be the dominant forms [13]. It can be readily demonstrated, see Fig. 13, that these cannot combine to form a suitable ribbon to nucleate stacking fault shear, which is thus absent despite a high resolved shear stress for $a\langle 1\,1\,2\rangle\{1\,1\,1\}$ slip.

5.2. Propagation of the stacking fault ribbon

The results indicate that nucleation of $a\langle 1\,1\,2\rangle\{1\,1\,1\}$ dislocation ribbons is in itself insufficient to ensure primary creep; it is possible for ribbons once nucleated to remain immobile through lack of sufficient shear stress to support their propagation. For example, the dislocation ribbon shown in Fig. 12 shows clearly the difficulty in propagating the stacking fault ribbons across the γ' precipitates. The threshold tensile stress of $\sim$530 MPa observed for the specimens in series A for deformation at 750 °C translates into

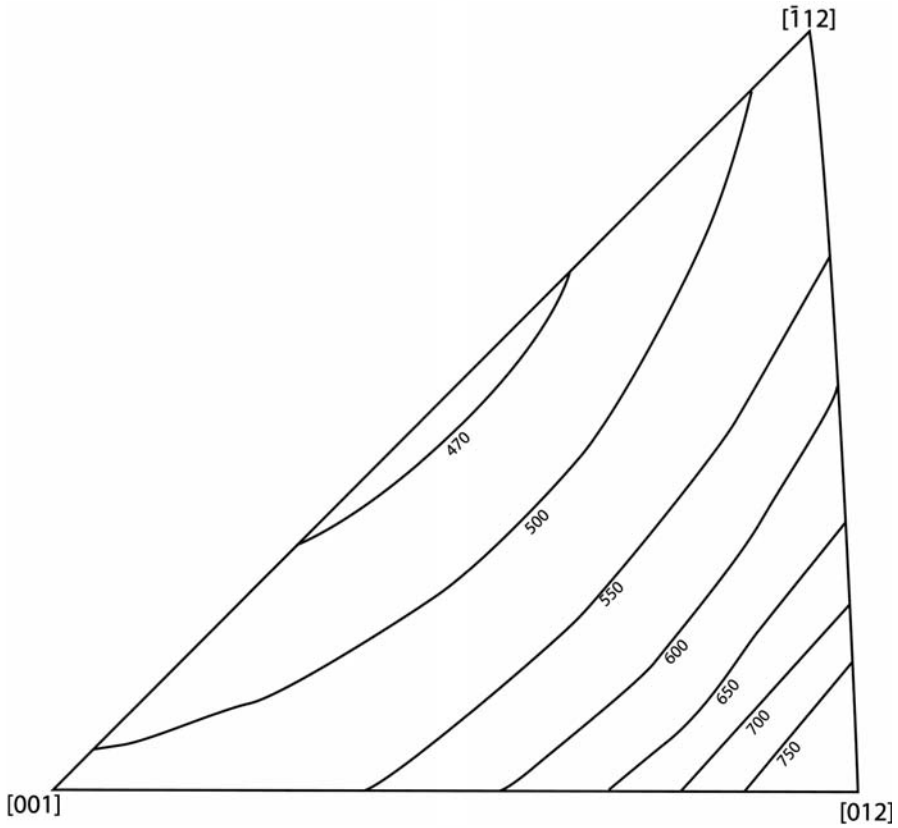

Fig. 14. Contour plot showing the orientations where nucleation of $a\langle 1\,1\,2\rangle$ ribbons becomes possible at the indicated applied stress levels. A stress threshold τ_{110} of 210 MPa is assumed.

a resolved shear stress on the primary $a\langle 1\,1\,2\rangle\{1\,1\,1\}$ slip system of 265 MPa. This value is broadly consistent with previous work on the creep mechanisms in specimens deformed at stresses below 500 MPa where stacking fault shear is not the operative mechanism [14,15]. Since the entry into the γ' requires the formation of intrinsic and extrinsic stacking faults, the value of the threshold is likely to vary with alloy composition and may involve the diffusion of stabilising elements to the faults [13]. Furthermore, there will be some dependence with temperature as the results indicate; these would suggest that stacking fault shear could occur at temperatures higher than 850 °C if the applied stress is sufficient.

In Fig. 15, orientations at which any one $a\langle 1\,1\,2\rangle\{1\,1\,1\}$ system has a resolved shear stress, denoted τ_{112}, in excess of 265 MPa are plotted as a function of the applied tensile stress. One can see that the contours mirror those for the Schmid factor for the primary slip system [9], being centred on the $[\bar{1}\,1\,8]$ pole and spreading from it to cover all orientations approximately equidistant from [0 0 1] as the stress increases. If this criterion for the propagation of the particular $a\langle 1\,1\,2\rangle\{1\,1\,1\}$ systems is combined with the nucleation criterion of Fig. 14, the overall effect of stress on the orientation dependence of $a\langle 1\,1\,2\rangle\{1\,1\,1\}$ of shear is then as depicted in Fig. 16. Note that the orientations where $a\langle 1\,1\,2\rangle\{1\,1\,1\}$ shear is predicted to operate are not the intersection of the two previous plots, Figs. 14 and 15, because the slip systems nucleated are not necessarily those with the highest resolved shear stress. Despite the caution which must be urged since the values of the two stress thresholds τ_{110} and τ_{112} are only approximate, important points emerge. Orientations close to [0 0 1] and towards the [0 0 1]–$[\bar{1}\,1\,2]$ diagonal are those for which substantial primary creep is predicted to occur; for these orientations, controlled. But towards [0 1 2], primary creep is controlled by nucleation nucleation is not problematical and primary creep is propagation controlled. But towards [0 1 2], primary creep is controlled by nucleation rather than by propagation.

The macroscopic dependence of the strain rate on the stress must, to some extent, translate to an effect of the resolved shear stress on the strain rate produced by individual slip systems. For example, the Schmid factor for $a\langle 1\,1\,2\rangle\{1\,1\,1\}$ shear increases from 0.471 at [0 0 1] to 0.5 at $[\bar{1}\,1\,8]$ some 10 °C away; a stress exponent of $n = 22$ increases the strain rate on the primary system by a factor of 3.7 simply as result of the increased Schmid factor. Interestingly, the reported primary creep rates at two very similar orientations, specimens 7 and 13 of Leverant and Kear's paper [10], give a ratio of 3.7. Orientations L and A have similar Schmid factors which, using the $n = 22$ exponent, predict a difference in strain rate of only 5%; consequently they show very similar primary creep and maximum strain rates.

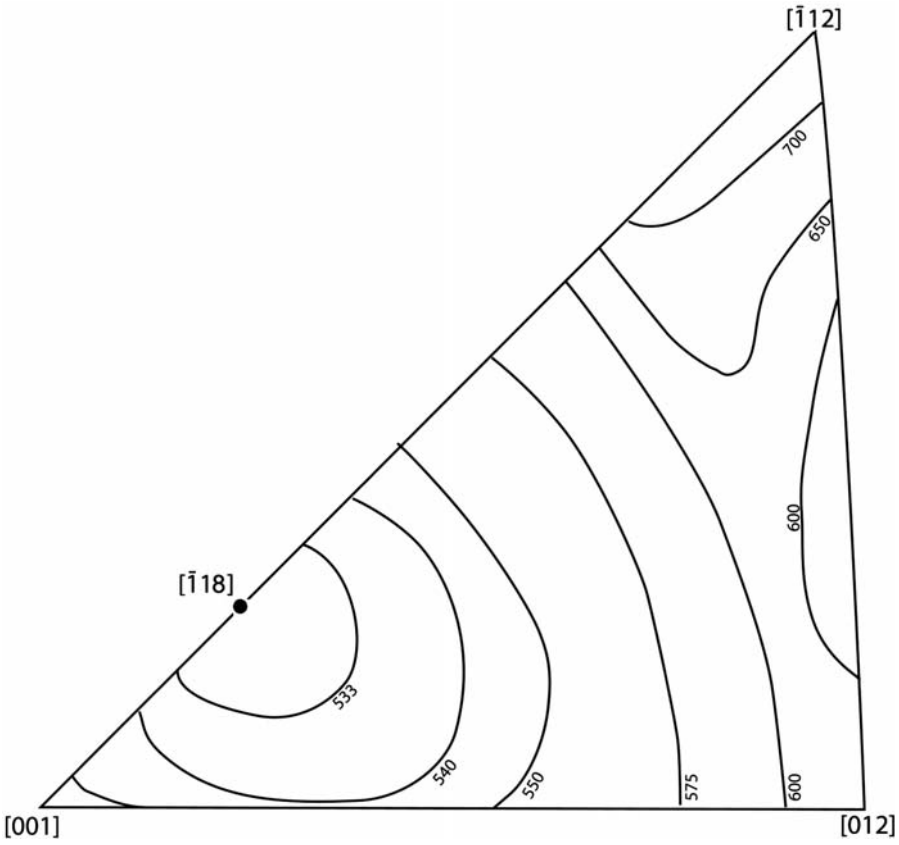

Fig. 15. Contour plot showing the orientations where propagation of $a\langle 1\,1\,2\rangle$ ribbons becomes possible at the indicated applied stress levels. A stress threshold τ_{112} of 265 MPa is assumed.

5.3. Hardening through dislocation interactions

The role of nucleation and propagation of $a\langle 1\,1\,2\rangle\{1\,1\,1\}$ ribbons in creep deformation has been emphasised, but the creep curves of Fig. 5 confirm that primary creep gives way eventually to a secondary mode during which the creep strain rate is approximately constant [5]. This implies that at least one mechanism of work-hardening is operative. Two potential sources of hardening are possible: interactions (i) between multiple $a\langle 1\,1\,2\rangle\{1\,1\,1\}$ systems [10,11], and (ii) between the $a\langle 1\,1\,2\rangle$ ribbons and the developing $a/2\langle 1\,1\,0\rangle$ dislocation networks surrounding the γ' precipitates [12,16]. These two possibilities are now discussed in turn.

The probability of interactions between $a\langle 1\,1\,2\rangle\{1\,1\,1\}$ ribbons can be quantified in several ways; MacKay and Meier [11] suggest that the degree of rotation, α, on the primary system needed to reach the [0 0 1]–[0 1 2] symmetry boundary determines the amount of primary creep strain. This criterion predicts contours of equal primary creep strain lying parallel to the [0 0 1]–[0 1 1] symmetry boundary and increasing as the orientation moves away from it, see Fig. 17. An alternative is to use the ratio of the Schmid factors on the primary and secondary systems as a measure of their relative activities and therefore the probability of work-hardening interactions, see Fig. 18. The ratio of the strain rates predicted using the stress exponent $n = 22$ for each contour are shown in brackets; this reaches a maximum of 6.3 close to the [0 0 1]–[$\bar{1}$ 1 2] boundary. Thus both approaches indicate that orientations close to the [0 0 1]–[0 1 2] symmetry boundary show rapid hardening because two $a\langle 1\,1\,2\rangle\{1\,1\,1\}$ systems are equally stressed. The ratio approach shows a more extensive area close to [0 1 2]. Very close to the [0 0 1] pole two additional slip systems come into play, further increasing the dislocation interactions. For orientations within the [0 0 1]–[$\bar{1}$ 1 2]–[0 1 2] triangle, the primary and secondary systems operate on different 111 planes and hence will interact frequently.

An important difference between shear on $a\langle 1\,1\,2\rangle\{1\,1\,1\}$ and $a/2\langle 1\,1\,0\rangle\{1\,1\,1\}$ slip systems is that the former is able to pass through the matrix without leaving dislocation debris; on the other hand the $a/2\langle 1\,1\,0\rangle$ dislocations leave dislocation loops around the γ' precipitates as they percolate through the γ/γ' structure [13]. It is postulated that dislocation activity in the γ must contribute to the hardening processes occurring and thus the slowing of the primary creep mechanism. The evolution of the primary creep strain can be followed by plotting the strain rate against time for a number of orientations each tested at 750 MPa, see Fig. 19. Those most favourably placed for shear, A, K and L, show an early and rapid increase in strain rate, specimen M taking longer to build up shear, possibly because the nucleation rate is slow. Specimen N, which deforms by $a/2\langle 1\,1\,0\rangle\{1\,1\,1\}$ deformation alone [12], shows a slight

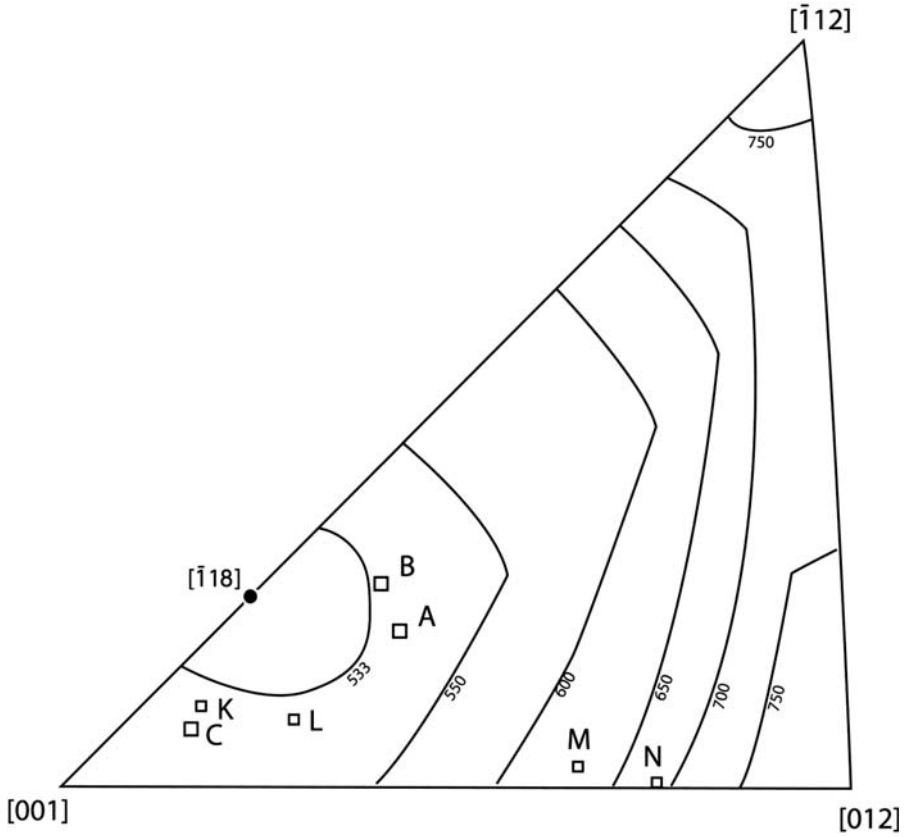

Fig. 16. Contour plot of orientations where the nucleation and propagation of $a\langle 1\,1\,2\rangle$ ribbons is possible as a function of stress assuming the stress threshold τ_{110} of 210 MPa and τ_{112} of 265 MPa.

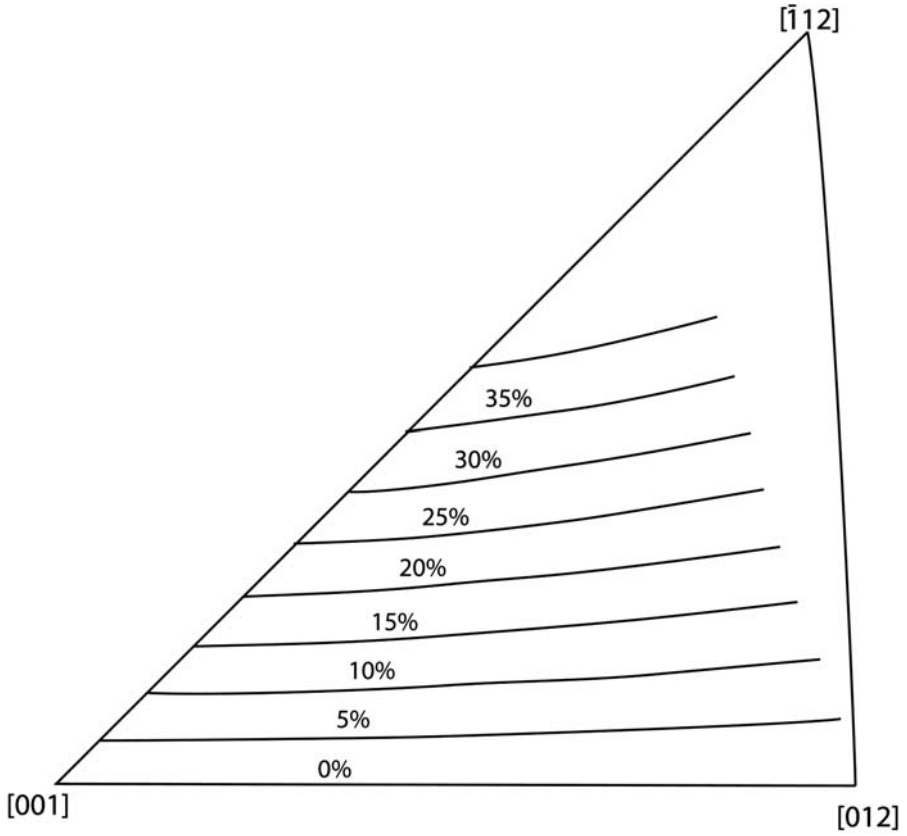

Fig. 17. Contour plot of lines of equal primary creep assuming that the rotation distance to the symmetry boundary determines the primary creep strain.

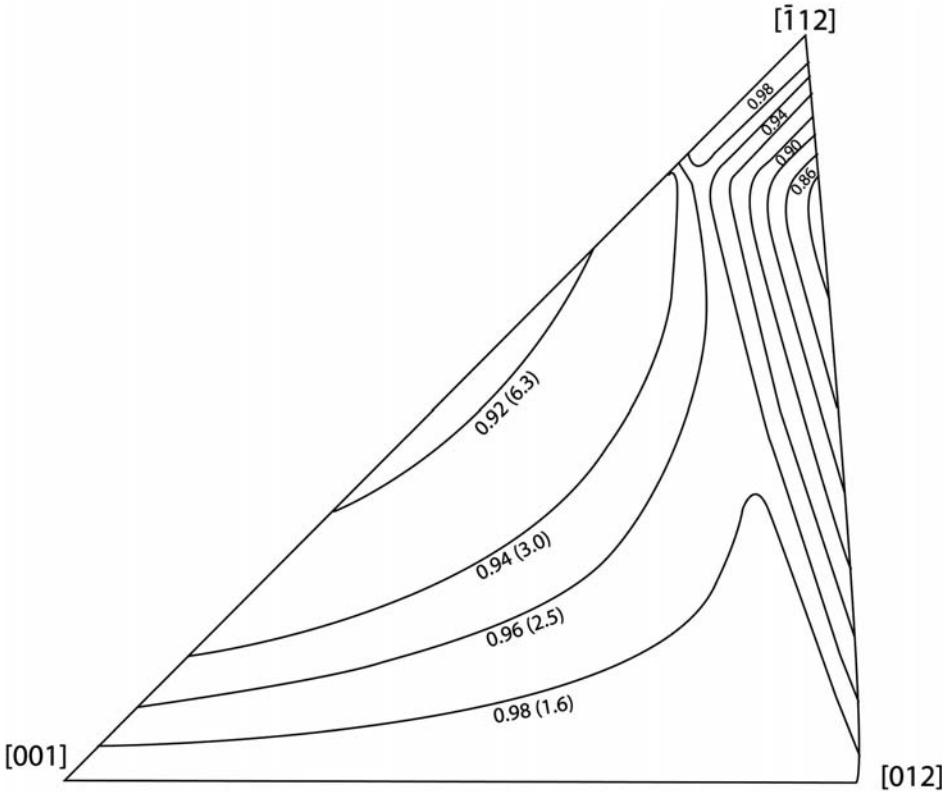

Fig. 18. Contour plot of the ratio of stress on the secondary $a\langle 1\,1\,2\rangle$ slip system to the stress on the primary system; areas where the ratio is close to 1 should show frequent interactions between $a\langle 1\,1\,2\rangle$ ribbons. Note that the numbers in brackets are estimates of the relative strain rates on the primary and secondary systems.

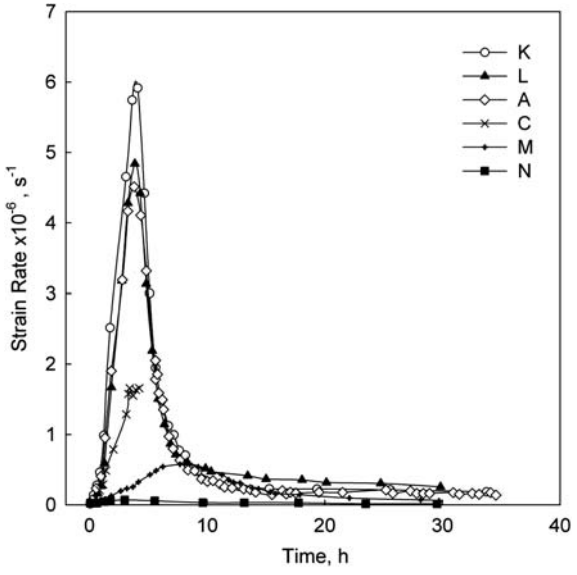

Fig. 19. Plot of strain rate vs. time for specimens of various orientations deformed at 750 °C and 750 MPa showing the similar time envelope.

peak at an early stage and drops to a low level after 20 h. However, all the curves fall within the same time envelope, indicating that, despite the large differences in strain, the processes ending primary creep for A, K, L and M take place during the first 20 h independent of the primary creep strain. If interactions between $a\langle 1\,1\,2\rangle\{1\,1\,1\}$ systems were the principal hardening mechanism, the orientation L, being closer to the [0 0 1] pole, should harden more rapidly than orientation A. Both start with the same resolved shear stress. The close agreement in the time to the end of primary creep suggests an underlying process which is less sensitive to orientation and which is the major cause of the transition to secondary creep. It is suggested that this process is the movement of the $a/2\langle 1\,1\,0\rangle$ dislocations in the γ. Where $a/2\langle 1\,1\,0\rangle$ deformation is the principal mechanism of creep at higher temperatures, orientation anisotropy is almost absent [5]. Interactions between the $a\langle 1\,1\,2\rangle$ ribbons clearly do occur and must contribute to the build up of dislocation density, increasing the work-hardening rate in orientations where multiple systems have a high resolved shear stress. However, the chances of these processes ending primary creep so uniformly for specimens in which the strains differ substantially seems to the present authors to be unlikely.

Should the principal mechanism of hardening be the interaction of $a\langle 1\,1\,2\rangle\{1\,1\,1\}$ dislocation ribbons with $a/2\langle 1\,1\,0\rangle$ $\{1\,1\,1\}$ dislocation debris, it follows that any process impeding the movement of $a/2\langle 1\,1\,0\rangle$ dislocations in the γ will delay the onset of secondary creep and thus increase the primary creep strain accumulated. This does indeed seem to occur. For example, the reduction in the γ channel width [16] and the presence of secondary precipitates

[17,18] have both been demonstrated to increase dramatically the extent of primary creep. Furthermore, the trend in alloy design to increase the resistance to tertiary creep at temperature beyond 850 °C has led inevitably to alloys exhibiting increasing levels of primary creep and thus creep anisotropy at temperatures of around 800 °C [19].

6. Rationalisation of primary creep dependence near ⟨0 0 1⟩

With this work, a rationalisation of the near-⟨0 0 1⟩ orientation dependence of primary creep in these materials has emerged, see Fig. 20. Whether $a\langle 1\,1\,2\rangle$ shear occurs or not depends crucially upon both the applied stress level and the orientation of the tensile axis. Nucleation is favoured by orientations along the [0 0 1]–[$\bar{1}$ 1 1] symmetry boundary, a region overlapping to some extent, but not completely, with the maximum resolved shear stress on the $a\langle 1\,1\,2\rangle\{1\,1\,1\}$ slip system. At moderate stress levels this area extends down towards [0 0 1]. Along the [0 0 1]–[0 1 1] symmetry boundary, work-hardening is rapid, as a result of both the propagation of $a/2\langle 1\,1\,0\rangle$ dislocations due to the maximum in the resolved shear on these dislocations, and of the interactions between $a\langle 1\,1\,2\rangle\{1\,1\,1\}$ systems. Orientations lying close to [0 1 2] and extending up towards [$\bar{1}$ 1 2] are predicted to demonstrate very low creep rates on each of the criteria: small probability of nucleation, low propagation rates and, should any $a\langle 1\,1\,2\rangle\{1\,1\,1\}$ deformation have occurred, rapid work-hardening. Of course, the results of the calculations presented here are sensitive to the values of the stress thresholds assumed; these are not well defined at present and are likely to vary with alloy composition, and also within an alloy from dendrite core to interdendritic regions. Further work is required to refine the calculations and to make a more sophisticated model of these effects, but the ideas outlined in this paper provide the basis for this.

7. Conclusions

The following conclusions can be drawn from this work:

1. Tensile creep tests on specimens of CMSX-4 single crystal superalloy of identical orientation within 20 °C of ⟨0 0 1⟩ have demonstrated conclusively that there is a threshold stress which must be exceeded before a detectable amount of primary creep is observed.
2. The sensitivity of the primary creep strain to the magnitude of the applied stress diminishes with increasing temperature. Part of the orientation dependence of primary creep can be accounted for by the variation of the resolved shear stress on the primary slip planes.
3. It is demonstrated unambiguously that the onset of primary creep deformation is associated with the propagation of $a\langle 1\,1\,2\rangle$ dislocation ribbons which are able to cut through both γ and γ', by a process which is referred to as stacking fault shear.
4. The $a\langle 1\,1\,2\rangle$ ribbons are nucleated from the $a/2\langle 1\,1\,0\rangle$ dislocations active in the γ matrix. Stacking fault shear and thus primary creep cannot occur when this mechanism is inoperative: i.e. at low levels of applied stress or at orientations where nucleation is suppressed because suitable combinations of Burgers vector are inactive.

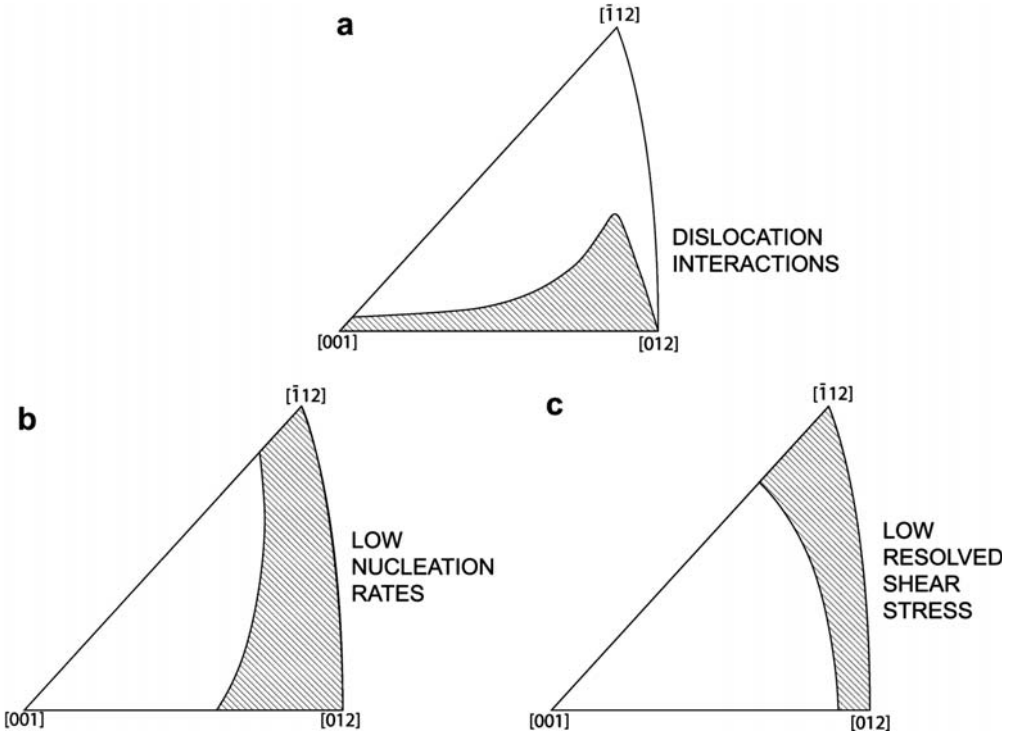

Fig. 20. Illustration of the factors contributing to the anisotropy of primary creep, for orientations close to the ⟨0 0 1⟩ direction.

5. The major source of work-hardening is the gradual filling of the γ channels with $a/2\langle 1\,1\,0\rangle$ dislocations; when this mechanism is impeded, primary creep is promoted. Interactions between the $a\langle 1\,1\,2\rangle$ ribbons may also contribute to hardening to some degree.
6. Primary creep is a process involving the nucleation, propagation and termination of mobile $a\langle 1\,1\,2\rangle$ dislocation ribbons: it is only by acknowledging the importance of these three effects that a rationalisation of the dependence on misorientation away from $\langle 0\,0\,1\rangle$ becomes possible.

Acknowledgments

The authors are grateful for support and funding from the United Kingdom's Engineering and Physical Sciences Research Council (EPSRC) and Rolls-Royce plc. The authors are grateful to Mr. Tim Smeeton for performing some of the calculations used here.

References

[1] Reed RC. Superalloys: fundamentals and applications. Cambridge: Cambridge University Press; 2006.
[2] Green K, Pollock TM, et al., editors. Superalloys 2004. Warrendale (PA): The Minerals, Metals and Materials Society; 2004.
[3] Harrison GF. Proc Instn Mech Eng 1993;208:19–31.
[4] Kear BH, Oblak JM. Met Trans 1970;1:2477–86.
[5] Matan N, Cox DC, Carter P, Rist MA, Rae CMF, Reed RC. Acta Mater 1999;47:1549–63.
[6] Pollock TM, Argon AS. Acta Metall Mater 1994;42:1859–74.
[7] Pollock TM, Field RD. Dislocations and high temperature plastic deformation of superalloy single crystals. In: Nabarro FRN, Duesbery MS, editors. Dislocations in solids, vol. 11. Amsterdam: Elsevier; 2002. p. 549.
[8] Ghosh RN, Curtis RV, McLean M. Acta Metall Mater 1990;38:1977–92.
[9] Nabarro FRN, de Villiers HL. The physics of creep. London: Taylor and Francis; 1995.
[10] Leverant GR, Kear BH. Metall Trans 1970;1:491–8.
[11] MacKay RA, Meier RD. Met Trans A 1982;13:1747–54.
[12] Rae CMF, Matan N, Cox DC, Rist MA, Reed RC. Met Trans A 2000;31:2219–27.
[13] Rae CMF, Matan N, Reed RC. Mater Sci Eng A 2001;300:125–34.
[14] Pollock TM, Argon AS. Acta Metall Mater 1992;40:1–30.
[15] Sass V, Glatzel U, Feller-Kniepmeier M. Acta Mater 1996;44:1967–77.
[16] Caron P, Ohta Y, Nakagawa YG, Kahn T. In: Reichman S, Duhl DN, Maurer G, Antolovich S, Lund C, editors. Superalloys 1988. Warrendale (PA): The Minerals, Metals and Materials Society; 1988. p. 215–24.
[17] Hopgood A, Martin JW. Mater Sci Eng 1986;82:27–36.
[18] Kakehi K. Metall Trans A 1999;30:1249–59.
[19] Drew GL, Kakehi K, Reed RC, Rae CMF. In: Green K, Pollock TM, Reed RC, et al., editors. Superalloys 2004. Warrendale (PA): The Minerals, Metals and Materials Society; 2004. p. 127–36.
[20] British Standard UDC 629.7. The British Standards Institution, London; 1965.
[21] Goulette MJ, Spilling PD, Arthey RP. In: Gell M, Kortovich CS, et al., editors. Superalloys 1984. Warrendale (PA): The Metals and Materials Society; 1984. p. 167–76.
[22] Schneider W, Hammer J, Mughrabi H. In: Antolovich SD, Stusrud RW, MacKay RA, Anton DL, Khan T, Kissinger RD, et al., editors. Superalloys 1992. Warrendale (PA): The Metals and Materials Society; 1992. p. 589–98.
[23] Sass V, Schneider W, Mughrabi H. Scr Mater 1994;31:885–90.
[24] Link T, Feller-Kniepmeier M. Metall Trans A 1992;23:99–105.
[25] Kuttner T, Feller-Kniepmeier M. Scr Metall Mater 1994;30:1121–6.
[26] Karunaratne MSA, Cox DC, Carter P, Reed RC. In: Pollock TM, Kissinger RD, et al., editors. Superalloys. Warrendale (PA): The Metals and Materials Society; 2000. p. 263–72.